Utilize the Equivalent Magnetic Circuit and Magnet Coverage to Figure out the Magnetic Field of the Air Gap and Stator Tooth of an Axial Flux Permanent Magnet Generator

Thanh Nguyen Vu *‡, Tan Nguyen Viet *, Tuan Phung Anh*

*Department of Electrical Engineering, School of Electronic and Electrical Engineering, Hanoi University of Science and Technology, No. 1 Dai Co Viet Street, Bach Khoa ward, Hai Ba Trung district, Hanoi City, Vietnam

(thanh.nguyenvu@hust.edu.vn, tan.nv212313M@sis.hust.edu.vn, tuan.phunganh1@hust.edu.vn)

‡ Corresponding Author; First Author, No. 1 Dai Co Viet Street, Bach Khoa ward, Hai Ba Trung district, Hanoi City, Vietnam, Tel: +84 94 257 4994, thanh.nguyenvu@hust.edu.vn

Received: 08.10.2023 Accepted:04.12.2023

Abstract- Currently, there is a growing interest among scientists worldwide in the field of low-speed direct drives, namely in axial flux permanent magnet (AFPM) machines. In this paper use an magnetic equivalent circuit (MEC) method is used, which suggests taking into account the nonlinear properties of steel by using the characteristics ($\varphi = f(F)$) that are unique to each steel section and the leakage flux components that are close to the air gap region. After that, the methods and equations are developed for figuring out nonlinear magnetic circuits using the Piecewise Cubic Spline (PCS) interpolation method. In order to enhance the precision of the outcomes obtained from the equivalent model, incorporating novel content is suggested into the examination of magnet coverage using Fourier series analysis. The precision of the analytical results is compared with the outcomes derived by the finite element analysis (FEA) method.

Keywords Axial flux permanent magnet, AFPMG, MEC, magnet coverage, nonlinear magnetic circuits.

1. Introduction

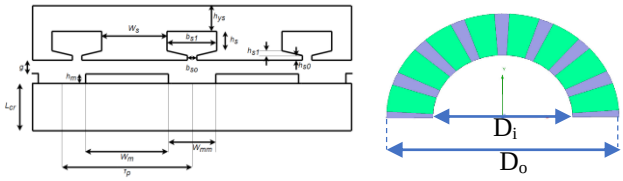
The AFPM machine comprises four distinct configurations: single-sided (SSSR), double-sided structure with double-rotor single-stator (TORUS) structure, double-sided structure with double-stator single-rotor (AFIR) structure, and a multi-disc machines with multi-rotor multi-stator (MSMR) structure. In recent times, there has been a significant utilization of AFPM generators in drive applications characterized by low speed and high torque, wherein the presence of a gearbox is unnecessary. Notable examples of such applications include wind turbine generators [3, 4] and submersible generators [22].

The computation of magnetic field distribution within electrical equipment, particularly AFPM generators, is critical to the overall design process [20]. Analytical approaches, reluctance network-based MEC methods, and FEA methods are all used to compute the magnetic field distribution in AFPM machines. The authors are classified depending on how they used analytical methodologies, as detailed in references [5-8]. The authors of [5] use a three-dimensional analytical approach based on magnetic scalar potential to investigate the distribution of magnetic flux density (MFD) in the air gap along the z-axis in a double-sided AFPM machine with the TORUS construction. To assess consistency, the acquired findings are compared to those produced using FEA. The authors of [6] investigated a slotted AFPM machine using a two-dimensional analytical modeling approach. The major goal was to calculate the cogging torque and electromagnetic torque using the Lorentz equation. The findings of the analysis are compared to the results of running the FEA model. In reference [7] the authors use a multi-slice analysis model that includes end-effects and a portion of the three-dimensional effects. This model is used to demonstrate the accuracy of cogging torque and open-circuit flux linkage computations. A study [8] used the Fourier series approach to spread out the

no-load magnetic field and the armature reactive magnetic field in an AFPM generator using an SSSR design. The principle of superposition can be used to calculate the resultant magnetic field. The references [9-15] and [16-19, 21] reveal that the authors of this study use the MEC method. Numerous scientists have expressed interest in this computational methodology. In comparison to FEA method, this method provides a substantial benefit in terms of significantly reduced computing time while retaining calculation accuracy within a suitable range of error. The authors of [9] established a MEC model for AFPM machines in order to evaluate their performance. The obtained results were validated using the FEA approach, resulting in a reasonable level of agreement. However, the paper does not provide detailed information about the equivalent magnetic circuit model and the iterative calculation algorithm. The authors of [10] used the MEC approach to analyze the AFPM machine model. They stated that this method allows for the determination of flux and torque distribution characteristics, which is especially useful in circumstances with high operating conditions. Nonetheless, the paper does not explain how they interpolate the magnetic permeability estimate based on the B-μ data of the SMC core and perform the iterative calculation procedure while studying nonlinear magnetic circuits. The authors of [11] employ a thorough analytical model that incorporates the solution of Maxwell's equations as well as a quasi-MEC-3D technique. This model is used to determine the distribution of the air gap flux density in the AFPM machine while it is not loaded. The analysis considers the impacts of slotting, end effects, and local saturation analyses of stator teeth. The outcomes are then compared to those obtained through FEM and experimental measurements. The authors of [12] examine and determine the performance of a flux-concentrating permanent magnet synchronous motor (PMSM) using a local nonlinear MEC in both the d- and q-axes. Nevertheless, the paper does not mention the relationship between magnetic flux density and relative nonlinear magnetic permeability in detail in the calculation. The authors of [13] used an analytical method that combines the quasi-3D mixed Maxwell equation and the MEC method for AFPM machines with the TORUS structure. This method allows for the quick and precise estimation of air-gap flux density and back EMF while accounting for the presence of leakage flux components. However, in the calculation, the author does not discuss in detail the relationship between magnetic flux density and relative nonlinear magnetic permeability; the paper does not mention solving the system of equations to calculate the flux, with the parameters being the nonlinear reluctance of the MEC model in the calculation algorithm. The authors of [14] investigate the AFPM machine used as a resolver. They provide the 3D-MEC method, which includes several critical features such as slot flux fringing, skewing slots, and static and dynamic rotor eccentricities. Although the paper does not explain how the core permeability μ of the input block is estimated. The piecewise cubic Hermite interpolating polynomial (PCHIP) was used by the authors of [15] to determine relative permeability. The suggested MEC approach is based on B-H curve data and incorporates the stator core permeability correction algorithm. Furthermore, the authors investigate the influence of slot opening on the air gap MFD and electromagnetic properties of the AFPM machine. The analytical method's results are compared to the FEM results obtained using JMAG software. It clear that getting the right interpolation values from discrete data that shows the relationship between magnetic flux density (B) and magnetic field strength (H) of steel is critical for ensuring that the MEC method works correctly when attempting to solve nonlinear parts of the reluctance network problem. The magnetic flux path, torque ripple, and back electromotive force (EMF) of an AFPM machine with an SSSR structure were investigated in [16]. The MEC and 3D-FEA methodologies were used for this investigation. Nonetheless, the MEC approach does not take magnetic circuit saturation into account. The authors of [17] presented a quasi-3D MEC model for an AFIR-structured AFPM machine. The analytical model takes into account a number of parameters, such as fringing flux, magnet-to-magnet flux leakage, slotting effect, and local saturation. The paper mentions the simple MEC model but not the solution with nonlinear reluctance. In [18], the authors used a quasi-3D MEC model to investigate the leakage flow coefficient of an AFPM machine with a slotless TORUS structure. Analytical computation of leakage flux components is performed by considering elements such as electrical machine size, permanent magnet material qualities, and magnetic saturation of the iron cor. To validate the proposed model's accuracy, the obtained results are compared using the recommended model to those obtained using the 3D FEM. The authors of [19] used the MEC method to examine yokeless and segmented armature AFPM machines. The MEC approach is well-known for its ability to rotate magnetization sources while maintaining constant resistance between the rotor and stator. The authors are able to anticipate the electromagnetic properties of electric machines using the proposed methodology. Furthermore, in the MEC model, the MFD of the permanent magnet is described using the corresponding Fourier series and is regarded as a source. Nonetheless, the effect of magnet coverage is not evaluated in the paper. The authors of proposed the ideal design of an AFPM machine with an AFIR structure in [21]. This concept is based on a quasi-3D MEC model that accounts for magnetic circuit saturation. The goal of the optimization task is to enhance the torque density of the machine while keeping its volume constant. The verification of optimal design outcomes is carried out using 3D-FEA analysis.

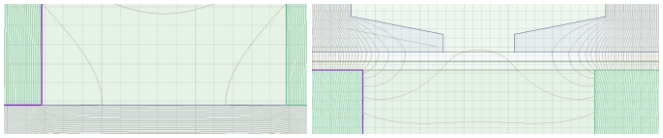
In this paper, the authors propose to use the Piecewise Cubic Spline (PCS) interpolation method [2] to precisely determine the nonlinear relationship between magnetic flux and magnetodynamic force ($\phi = f(F)$) of M800-50A steel in this investigation. This analysis was performed using Maple software [1]. The novel of the paper is shown in two parts: Firstly, analyze the influence of magnet coverage on the MFD distribution at the air gap using Fourier series, with a particular emphasis on the 3^{rd}, 5^{th}, and 7^{th} harmonic components. Secondly, propose a MEC method with a nonlinear analysis algorithm to calculate the air gap MFD (B_g) and the different leakage flux components at the tooth tips and stator tooth using results obtained from Fourier series analysis and PCS interpolation method. The acquired data are compared with the results of the FEA method, demonstrating the correctness of the proposed strategy.

2. Construction of a 2D MEC Model of an AFPM Machine



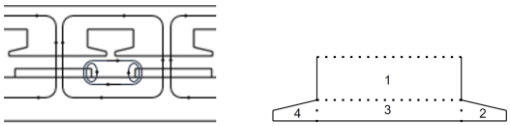
(a) (b)

Fig. 1. Dimensions of the AFPM generator, (a) 2D model, (b) Detailed dimensions are half of the rotor cutout.



(a) (b)

Fig. 2. Leakage magnetic flux, (a) magnet-to-rotor yoke flux leakage, (b) magnet-to-magnet flux leakage.



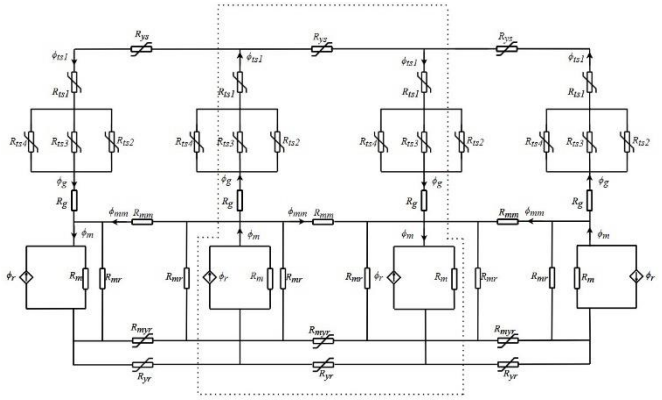
(a) (b)

Fig. 3. (a) Main flux path and leakage flux path, (b) Different reluctance regions of the tooth tip and tooth.

The tooth tip region is separated into three smaller portions because it has a peculiar shape with two narrow protrusions near the stator slot opening that easily saturate the magnetic circuit. The problem will be solved with such a division. Consider the magnetic saturation portion of the tooth tip.

The MEC diagram is obtained by modeling the magnetic circuit using a reluctance network with the magnetic flux lines shown in "Fig. 3a" and separating the tooth tip region in detail as shown in "Fig. 3b".

A closed flux loop is used to calculate the magnetic circuit diagram in "Fig. 3" with three magnetic flux loops. Considering one flux loop, the corresponding regions on the tooth, air gap, and magnet will be reduced by half, resulting in the magnetic flux source of the magnet (Φ_r) being determined according to formula (26), permanent magnet reluctance (Rm) being determined according to formula (27), air gap reluctance (Rg) being determined according to formula (28), and the reluctance components (R_{ts1}) and (R_{ts3}) being determined according to formula (29) and (30). As illustrated in "Fig. 5", the MEC design is obtained when considering a flux loop without considering the armature reaction.



Where: Nonlinear reluctance

Linear reluctance

Fig. 4. The MEC diagram.

Table 1. Equations for computing linear reluctances.

Reluctances	Equations	Reluctances	Equations
Air gap leakage reluctance between two adjacent magnets [15]	$R_{mm} = \frac{\pi}{\mu_o L_s ln(1+\frac{\pi g}{W_{mm}})}$ (1)	Leakage reluctance between the magnet and the rotor yoke [15]	$R_{mr} = \frac{\pi}{\mu_o L_s ln[1+\frac{\pi min(g,\frac{W_{mm}}{2})}{h_m}]}$ (2)
Reluctance of permanent magnets [17]	$R_m = \frac{h_{pm}}{\mu_o \mu_r L_s W_m}$ (3)	Air gap reluctance [17]	$R_g = \frac{g}{\mu_o W_g L_s}$ (4)

Table 2. Equations for computing non-linear reluctances

Reluctances	Equations	Reluctances	Equations
Reluctance of stator tooth	$R_{ts1} = \frac{h_s}{\mu_o \mu_s(B) L_s W_s}$ (5)	Similar to formula (1), rotor yoke leakage reluctance between two adjacent permanent magnets.	$R_{myr} = \frac{\pi}{\mu_o \mu_s(B) L_s ln(1+\frac{\pi l_{myr}}{W_{mm}})}$ (6)
Reluctance of portion 3 of stator tooth tip.	$R_{ts3} = \frac{l_{ts3}}{\mu_o \mu_s(B) W_s L_s}$ (7)	Reluctance of portion 2 of stator tooth tip.	$R_{ts2} = \frac{l_{ts2}}{\mu_o \mu_s(B) W_{ts} L_s}$ (8)
Rotor yoke reluctance.	$R_{yr} = \frac{l_{yr}}{\mu_o \mu_s(B) h_{yr} L_s}$ (9)	Stator yoke reluctance.	$R_{ys} = \frac{l_{ys}}{\mu_o \mu_s(B) h_{ys} L_s}$ (10)

		Reluctance of portion 4 of stator tooth tip.	$R_{ts4} = \frac{l_{ts4}}{\mu_o \mu_s(B) W_{ts4} L_s}$ (11)

Table 3. The detailed sizing equations relate to the different reluctance regions.

Parameters	Equations	Parameters	Equations
Axial length of the stator core [22]	$L_s = \frac{D_o - D_i}{2}$ (12)	Distance between two adjacent magnets [22]	$W_{mm} = \frac{\pi D_{avg}(1-\alpha_p)}{2p}$ (13)
The stator average diameter [22]	$D_{avg} = \frac{D_o + D_i}{2}$ (14)	Magnet width [22]	$W_m = \frac{\pi D_{avg} \alpha_p}{2p}$ (15)
Stator yoke height	$h_{ys} = L_s - h_{ts}$ (16)	Stator tooth height	$h_{ts} = h_o + h_1 + h_s$ (17)
Stator yoke average length	$l_{ys} = \frac{\pi D_{avg}}{Q}$ (18)	Width of air gap [22]	$W_g = W_m + 2k_c g$ (19)
Line length of magnetic flux portion 2.	$l_{ts2} = h_{s0} + h_{s1}$ (20)	Width of portion 2 through which the flux passes.	$W_{ts2} = \frac{1-\alpha_p}{2}\tau_p - \frac{b_{s0}}{2}$ (21)
Line length of magnetic flux portion 3.	$l_{ts3} = h_{s0} + h_{s1}$ (22)	Line length of magnetic flux portion 4.	$l_{ts4} = \sqrt{h_{s1}^2 + \left(\frac{b_{s1} - b_{s0}}{2}\right)^2}$ (23)
Width of portion 4 through which the flux passes.	$W_{ts4} = h_{s0} + h_{s1}$ (24)	The tooth width and the width of portion 3 through which the flux passes.	$W_s = \frac{\pi D_{avg}}{Q} - b_{s1}$ (25)

Table 4. Equations for computing the parameters of the reduced MEC diagram (see "Fig. 5b").

Equations	Equations
$\Phi'_r = B_r \frac{A_m}{2} = \frac{\Phi_r}{2}$ (26)	$R'_m = \frac{w_m}{\mu_r \mu_0 \frac{A_m}{2}} = 2\frac{w_m}{\mu_r \mu_0 A_m} = 2R_m$ (27)
$R'_g = \frac{g}{\mu_0 \frac{A_g}{2}} = 2\frac{w_m}{\mu_0 A_g} = 2R_g$ (28)	$R'_{ts1} = \frac{l_{ts1}}{\mu_r \mu_0 \frac{A_{ts1}}{2}} = 2\frac{l_{ts1}}{\mu_r \mu_0 A_{ts1}} = 2R_{ts1}$ (29)
$R'_{ts3} = \frac{l_{ts3}}{\mu_r \mu_0 \frac{A_{ts3}}{2}} = 2\frac{l_{ts3}}{\mu_r \mu_0 A_{ts3}} = 2R_{ts3}$ (30)	The 2nd loop equation (see "Fig. 5b") $F_{mm} = 2F_{em} + F_{myr}$ (31)
$R_{em} = \frac{R'_m R_{mr}}{R'_m + R_{mr}}$ (32)	The 1st loop equation (see "Fig. 5b") $2F_{ts3} = F_{mm} - 2F_g - 2F_{ts1} - F_{ys}$ (33)

Table 5. Equations to compute MFDs

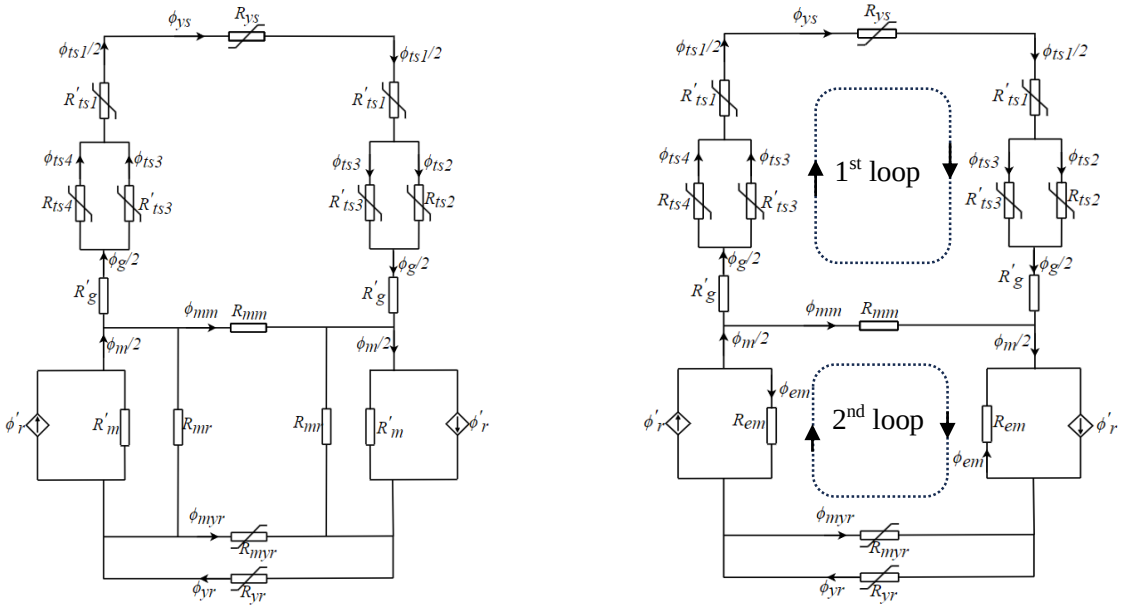
$\boldsymbol{B_g = \frac{\Phi_g}{L_s W_m}}$ (34)	$\boldsymbol{B_{ts1} = \frac{\Phi_{ts1}}{L_s h_s}}$ (35)	$\boldsymbol{B_{ts2} = \frac{\Phi_{ts2}}{L_s W_{ts2}}}$ (36)	$\boldsymbol{B_{ts3} = \frac{\Phi_{ts3}}{L_s W_s}}$ (37)	$\boldsymbol{B_{ts4} = \frac{\Phi_{ts4}}{L_s W_{ts4}}}$ (38)

3. Fourier Series Development to Analyse the Influence of Magnet Coverage

Magnet coverage is defined as the ratio of the width of the magnet to the width of the pole pitch $\alpha = \frac{W_m}{\tau_p}$ (as shown in "Fig. 1a"). To analyze the effect of magnet coverage on the air gap MFD (Bg), the air gap MFD is considered to be formed by permanent magnets to be an ideally rectangular waveform, as shown in "Fig. 6".

The magnetic field at the air gap is periodic with a 2π electric angle period and is characterized by the Fourier series with the flux density distribution function, which is as follows:

$$B(\theta)\begin{cases} B_g, & \left(\frac{\pi}{2}-\alpha\frac{\pi}{2}\right)\le\theta\le\left(\frac{\pi}{2}+\alpha\frac{\pi}{2}\right) \\ -B_g, & \left(\frac{3\pi}{2}-\alpha\frac{\pi}{2}\right)\le\theta\le\left(\frac{3\pi}{2}+\alpha\frac{\pi}{2}\right) \\ 0, & \left[0\le\theta<\left(\frac{\pi}{2}-\alpha\frac{\pi}{2}\right)\right]\&\left[\left(\frac{\pi}{2}+\alpha\frac{\pi}{2}\right)<\theta<\left(\frac{3\pi}{2}-\alpha\frac{\pi}{2}\right)\right]\&\left[\left(\frac{3\pi}{2}+\alpha\frac{\pi}{2}\right)<\theta\le 2\pi\right] \end{cases}$$



(a) (b)

Fig. 5. The MEC diagram MEC diagram when considered in a flux loop, (a) Original diagram, (b) Reduced diagram.

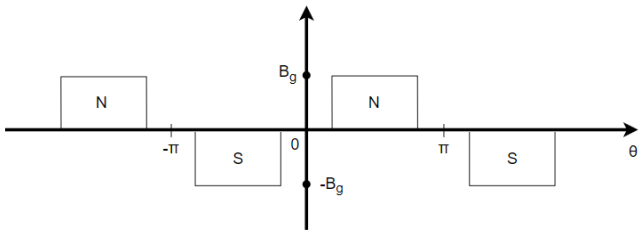


Fig. 6. Distribution of air gap MFD according to electric angle.

The results of the Fourier series according to magnet coverage α are as follows:

$$B(\theta)=\frac{4B_g}{\pi}\sum_{n=1}^{\infty}\frac{sin(n\frac{\pi}{2})\,sin(n\frac{\pi\alpha}{2})}{n}sin(n\theta)$$

$$=\frac{4B_g}{\pi}K_{n\alpha}\,sin(n\theta) \quad (39)$$

Define K_α as a coefficient based on the magnet coverage.

$$K_{n\alpha}=\sum_{n=1}^{\infty}\frac{sin(n\frac{\pi}{2})\,sin(n\frac{\pi\alpha}{2})}{n} \quad (40)$$

Table 6. Determine the Kα coefficient for the fundamental component and the 3rd, 5th, 7th harmonic components.

The magnet coverage	Fundamental component	3rd harmonic component	5th harmonic component	7th harmonic component
α	$K_{1\alpha}$	$K_{3\alpha}$	$K_{5\alpha}$	$K_{7\alpha}$
0.6	0.809	-0.103	-0.2	-0.044
0.65	0.852	-0.026	-0.184	-0.108
0.66	0.860742	-0.01047	-0.1782	-0.11815
0.67	0.868632	0.005236	-0.17053	-0.12625
0.68	0.876307	0.02093	-0.1618	-0.13283
0.69	0.883766	0.036578	-0.15208	-0.13779
0.7	0.891	0.052	-0.141	-0.1411
0.75	0.923	0.127	-0.076	-0.131

"Table 6." shows that the least 3rd harmonic value ($K_{3\alpha}$) is 0.005236. With this result, the equivalent magnet coverage is computed to be 0.67, which corresponds to the coefficient ($K_{1\alpha}$) of 0.868 of the fundamental components used in the design of the AFPM generator and determines the air gap MFD and other MFD components on the stator tooth.

As a result, the average of the fundamental component's air gap MFD is computed using the equation below.

$$B_g^{avg} = \frac{2}{\pi}\left(\frac{4B_g}{\pi}K_{1\alpha}\right) \quad (41)$$

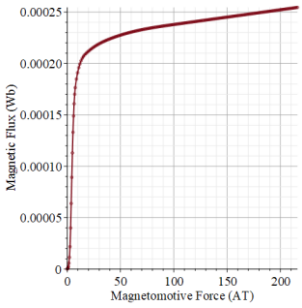
4. Create Interpolation Functions (ϕ = f(F)) for Nonlinear Reluctance Regions.

The discrete points of curve B = f(H) of M800-50A steel are transformed into discrete points of the curve ϕ = f(F) using the following formulas: $\phi = \frac{B}{S}$ and F = H.l

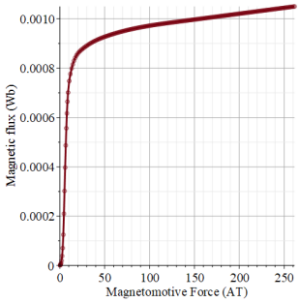
Because the discrete point of the curve ϕ = f(F) produces a severely nonlinear curve, the PCS interpolation method is used to provide highly accurate interpolated values. On each interpolated piecewise, the sub-function has the form $a(x-n)^3 + b(x-m)^2 + dx + e$. "Fig. 7" shows that there are a total of seven nonlinear reluctance regions: R_{ys}, R'_{ts1}, R'_{ts3}, R_{ts2}, R_{ts4}, R_{yr}, and R_{myr} create seven discrete curves ϕ = f(F). The corresponding interpolation curves ϕ = f(F) of the reluctance regions is obtained in "Fig. 7" by using the PCS interpolation method.

5. Determine the Air Gap MFD and Other MFD Components on the Stator Tooth.

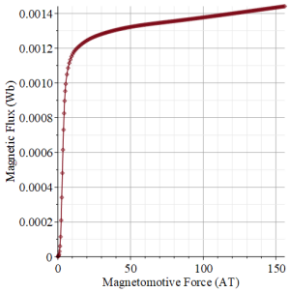
The analytical algorithm shown in "Fig. 8" is used to compute the air gap MFD (B_g^t). Firstly, utilizing Section 3, calculate the magnet coverage (α) in "Table 6." using Fourier series analysis. Section 3 shows that the magnet coverage value is chosen to minimize the 3rd harmonic component, which corresponds to the α coefficient of 0.67.



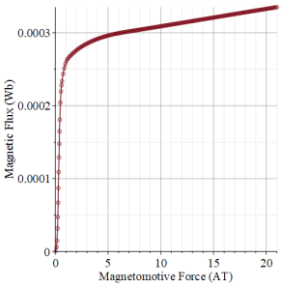
Curve ϕ_{myr} = f(F_{myr}) (a)



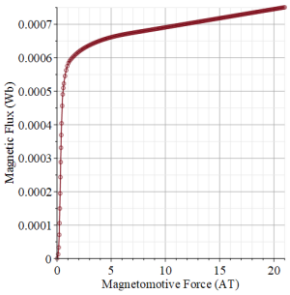
Curve ϕ_{yr} = f(F_{yr}) (b)



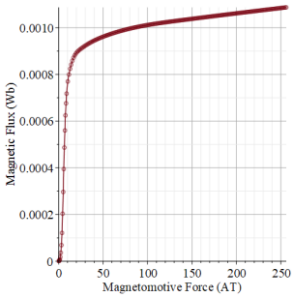
Curve ϕ_{ts1} = f(F_{ts1}) (c)



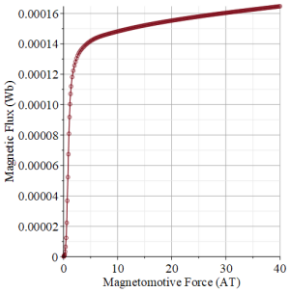
Curve ϕ_{ts2} = f(F_{ts2}) (d)



Curve ϕ_{ts3} = f(F_{ts3}) (e)



Curve ϕ_{ys} = f(F_{ys}) (f)



Curve ϕ_{ts4} = f(F_{ts4}) (g)

Fig. 7. Interpolation curves of seven nonlinear reluctance regions.

In step 2, determine the linear reluctance values R_{mm}, R_{mr}, R'_m, R'_g, and R_{em} using formulas (1), (2), (27), (28) and (32) (see "Table 7.") and the nonlinear reluctances R_{ts1}, R_{myr}, R_{ts3}, R_{ts2}, R_{yr}, R_{ys}, and R_{ts4} using formulas (5), (6), (7), (8), (9), (10), and (11) (see "Table 8.").

Table 7. Results of linear reluctances.

Reluctances	Values	Unit
Between two adjacent magnets (R_{mm})	233211382	AT/Wb
Leakage reluctance between the magnet and the rotor yoke (R_{mr})	218048417	AT/Wb
Permanent magnets (R'_m)	15211066	AT/Wb
Air gap (R'_g)	1338756	AT/Wb
Equivalent reluctance (R_{em})	14219138	AT/Wb

Table 8. Results of nonlinear reluctances.

Reluctances	Values	Unit
Stator yoke (R_{ys})	26083	AT/Wb
Rotor yoke (R_{yr})	27070	AT/Wb
Rotor yoke leakage reluctance between two adjacent permanent magnets (R_{myr})	159795	AT/Wb
Stator tooth (R_{ts1})	22175	AT/Wb
Portion 2 of stator tooth tip (R_{ts2})	9878	AT/Wb
Portion 3 of stator tooth tip (R_{ts3})	2206	AT/Wb
Portion 4 of stator tooth tip (R_{ts4})	25425	AT/Wb

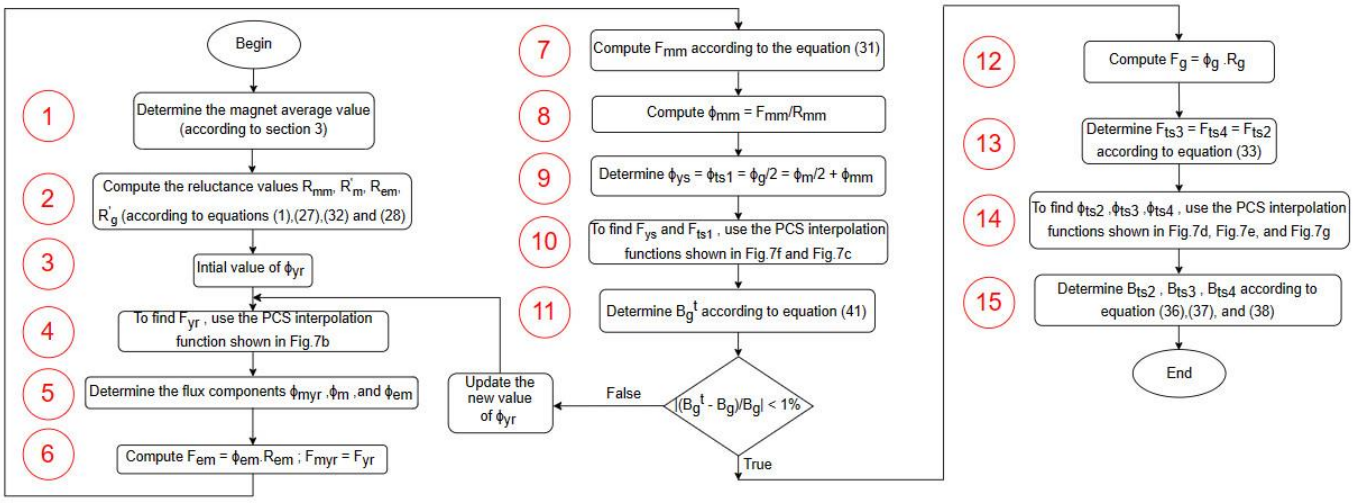


Fig. 8. The air gap MFD (B_g^t) is calculated using an analytical algorithm.

In step 3, initialize the initial ϕ_{yr} value, and after many iterative steps by checking the error of the air gap MFD value (B_g^t), determine ϕ_{yr} to be 0.000486 (Wb).

In step 4, use the PCS interpolation function to determine magnetomotive force (MMF) (F_{yr}) equal to 6.6151 (AT).

In step 5, use the PCS interpolation function to determine the flux component (ϕ_{myr}) equal to 0.000163 (Wb) and calculate the flux components (ϕ_m and ϕ_{em}) using Kirchhoff's Flux Current Law formulated for node, as shown in "Table 9.".

Table 9. Results of flux components.

Flux	Values	Unit
ϕ_m	0.001298	Wb
ϕ_{em}	0.0000608	Wb

In step 6, use the formula $F_{em} = \phi_{em}R_{em}$ to determine the MMF (F_{em}). Because the two reluctances, R_{myr} and R_{yr}, are parallel, F_{myr} is equal to F_{yr}.

In step 7, calculate the F_{mm} component as 1734 (AT) using Kirchhoff's Magnetic Voltage Law formulated for the 2nd loop (see "Fig. 5b").

In step 8, calculate the flux component ($\phi_{mm} = \frac{F_{mm}}{R_{mm}}$), which is equal to 0.00000743 (Wb).

In step 9, calculate the flux components (ϕ_{ys}, ϕ_{ts1}, and ϕ_g) using Kirchhoff's Flux Current Law formulated for node, as shown in "Table 10.".

Table 10. Results of flux components.

Flux	Values	Unit
ϕ_{ys}	0.0006418	Wb
ϕ_{ts1}	0.0006418	Wb
ϕ_g	0.0012836	Wb

In step 10, use the PCS interpolation function to determine the MMFs (F_{ys} and F_{ts1}), as shown in "Table 11."

Table 11. Results of MMFs.

MMF	Values	Unit
F_{ys}	7.886	AT
F_{ts1}	3.628	AT

In step 11, calculate the air gap MFD (B_g^t) according to equation (41); afterthat, check the error in the air gap MFD (B_g^t) value. If the error is outside the range of ±1%, go back to step 4 to update ϕ_{yr} again. If correct, go to step 12.

In step 12, using the formula $F_g = \phi_g.R_g$, determine the air gap MMF (F_g) equal to 859.286 (AT).

In step 13, the magnetic flux pairs (ϕ_{ts2} and ϕ_{ts3}, ϕ_{ts3} and ϕ_{ts4}) all cause equal MMFs, respectively. Kirchhoff's Magnetic Voltage Law is written for the 1st loop (see "Fig. 5b") to determine MMF (F_{ts3}) using formula (33). Because the three reluctances, R'_{ts3} and R_{ts2} and R_{ts4}, are parallel, F_{ts2} and F_{ts4} are equal to F_{ts3}, as shown in "Table 12.".

Table 12. Results of MMFs.

MMF	Values	Unit
F_{ts3}, F_{ts2}, F_{ts4}	0.461788	AT

In step 14, use the PCS interpolation functions to find the fluxes (ϕ_{ts2}, ϕ_{ts3}, and ϕ_{ts4}) from the MMFs (F_{ts2}, F_{ts3}, and F_{ts4}), respectively, as shown in "Table 13."

Table 13. Results of flux components.

Flux	Values	Unit
ϕ_{ts2}	0.0000939	Wb
ϕ_{ts3}	0.0005359	Wb
ϕ_{ts4}	0.0001474	Wb

In step 15, calculate the MFD values at the tooth tip portions B_{ts2}, B_{ts3}, and B_{ts4} according to equations (36), (37), and (38), respectively, as shown in "Table 14.".

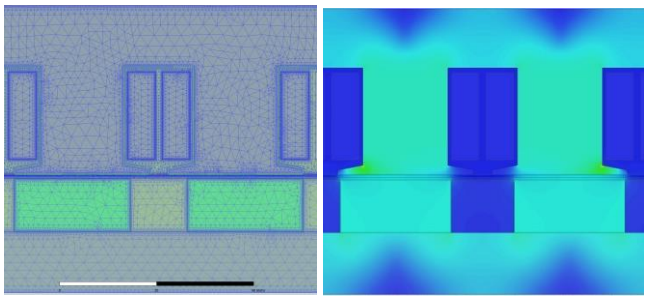
Table 14. Results of MFD values.

MFD	Values	Unit
B_{ts2}	0.561	T

B_{ts3}	1.42	T
B_{ts4}	1.62	T

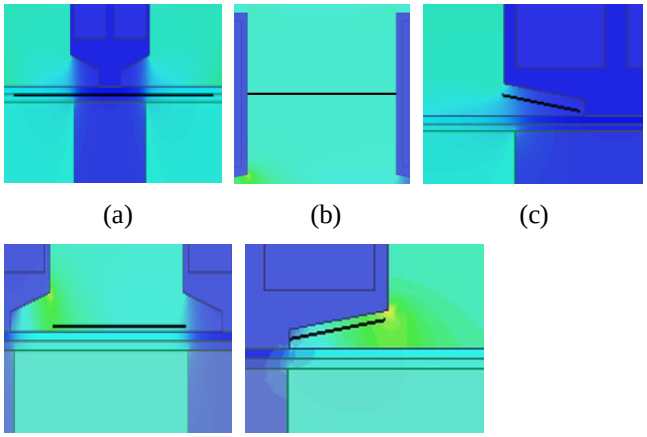
6. Conduct a Simulation and Verify the Analytical Results.

To ensure that the MEC method and magnet coverage (α) analysis provided reliable results, the results are compared to those obtained from the FEA software. The following are the simulation results:



(a) (b)

Fig. 9. The AFPM generator 2D model, meshing (a), MFD distribution (b).



(a) (b) (c)

(d) (e)

Fig. 10. MFD distribution at the air gap (a) and in various portions of the tooth tip: portion 1 (b), portion 2 (c), portion 3 (d), and portion 4 (e).

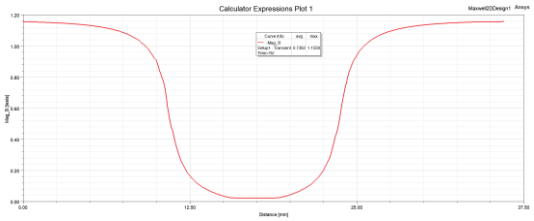


Fig. 11. Average MFD at the air gap, Bavg = 0,738 (T)

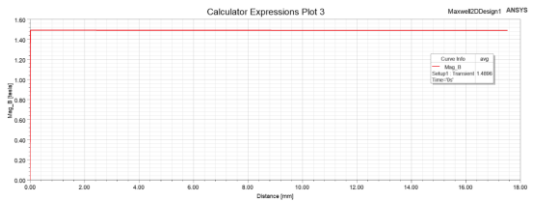


Fig. 12. Average MFD of tooth in portion 1, Bavg = 1,49 (T).

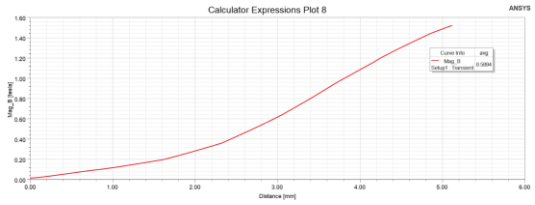


Fig. 13. Average MFD of tooth in portion 2, Bavg = 0,59 (T).

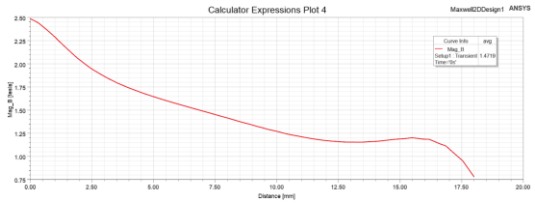


Fig. 14. Average MFD of tooth in portion 3, Bavg = 1,47 (T).

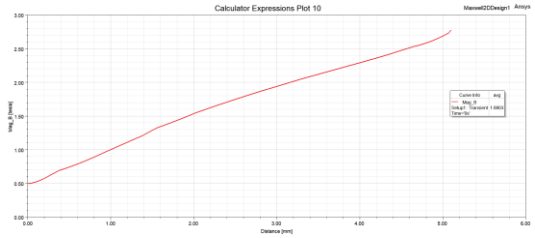


Fig. 15. Average MFD of tooth in portion 4, Bavg = 1,69 (T).

The results of calculating the average magnetic flux density at the air gap, stator tooth, and stator tooth tips by 2D FEA analysis are compared with the results of analytical calculations using the MEC method combined with Fourier series analysis of magnet coverage. The results show that the largest relative error is less than 5%, within the allowable error limit, as shown in "Table 15.". This result shows that the analytical method has quite high accuracy with a much faster calculation time than the FEA-2D analysis method.

Table 15. Compare the results of determining MFDs using analytical analysis and FEM methods.

Magnetic flux density	Analytical analysis values	FEA values	Unit	Relative error (%)
Air gap B_g^{avg}	0.745	0.738	T	-0.91
Stator tooth (B_{ts1})	1.54	1.49	T	-3.35
Portion 2 of the stator tooth tip (B_{ts2})	0.561	0.59	T	1.7
Portion 3 of the stator tooth tip (B_{ts3})	1.42	1.47	T	3.4
Portion 4 of the stator tooth tip (B_{ts4})	1.62	1.69	T	4.14

7. Conclusion

In this paper, the air gap MFD as well as the MFD in the tooth tip and tooth have been analyzed and computed. The results are acquired by combining a MEC method with three

related contents proposed by the authors. The first content is a high-accuracy nonlinear curve interpolation function of steel ($\phi = f(F)$) based on the PCS interpolation method. The second content is to select the magnet coverage (α) based on its influence on the MFD distribution at the air gap when high-order harmonic components are taken into account. The analytical algorithm for finding nonlinear solutions to the MEC model is the third piece of content. When these analytical results are compared to the 2D FEA results, the analytical results have a reasonably modest error of less than 5% (as shown in "Table 15."). The most significant advantage realized is that the computation time utilizing the MEC method is significantly reduced when compared to the 2D FEA method, with the relative error remaining within the permissible range.

Acknowledgments

This research is funded by Hanoi University of Science and Technology (HUST) under project number T2022-PC-008

References

[1] F. Garvan, The Maple Book, Chapman & Hall/CRC, 2002. (Book)

[2] E. Kreyszig, H. Kreyszig, E. J. Norminton, Advanced Engineering Mathematics, JOHN WILEY & SONS, INC, 10th edition, 2011. (Book)

[3] K. Wirtayasa, C. Hsiao, "Performances comparison of axial-flux permanent magnet generators for small-scale vertical-axis," Alexandria Engineering Journal, p. 61, 3 July 2021, doi: https://doi.org/10.1016/j.aej.2021.06.074. (Article)

[4] S. Kim, J. Li, D. Choi, Y. Cho, "Design and analysis of axial flux permanent magnet generator for direct-driven wind turbines," International Journal of Power Systems, vol. 2, 2017. (Article)

[5] Y. K Huang, B. Y. Ge, J. N. Dong, H. Y. Lin, J. G. Zhu, and Y. G. Guo, "3-D analytical modeling of no-Load magnetic field of ironless axial flux permanent magnet machine," IEEE Transactions on Magnetics, vol. 48, No. 11, pp. 2929-2932, November 2012, doi: 10.1109/TMAG.2012.2194699. (Article)

[6] S. T. Boroujeni, A. A. Mohammadi, A. Oraee, and H. Oraee, "Approach for analytical modelling of axial-flux PM machines," IET Electric Power Applications, vol. 10, No. 6, pp. 441-450, 01 July 2016, doi: https://doi.org/10.1049/iet-epa.2015.0645. (Article)

[7] H. Tiegna, Y. Amara, and G. Barakat, "A new quasi-3-d analytical model of axial flux permanent magnet machines," IEEE Transactions on Magnetics, vol. 50, No. 2, 26 February 2014, doi: 10.1109/TMAG.2013.2285739. (Article)

[8] T. F. Chan; L. L. Lai; S. Xie, "field computation for an axial flux permanent-magnet synchronous generator," IEEE Transactions on Energy Conversion, vol. 24, No. 1, 06 February 2009, doi: 10.1109/TEC.2008.2011830. (Article)

[9] Y. K. Huang, T. Zhou, J. N. Dong, H. Y. Lin, H. Yang, and M. Cheng, "Magnetic equivalent circuit modeling of yokeless axial flux permanent magnet machine with segmented armature," IEEE Transactions on Magnetics, vol. 50, No. 11, pp. 1-4, November 2014, doi: 10.1109/TMAG.2014.2322874. (Article)

[10] Y. Kano, T. Kosaka, and N. Matsui, "A simple nonlinear magnetic analysis for axial-flux permanent-magnet machines," IEEE Transactions on Industrial Electronics, vol. 57, No. 6, pp. 2124–2133, 20 October 2009, doi: 10.1109/TIE.2009.2034685. (Article)

[11] W. Tong, S. Wang, S. Wu and R. Tang, "A complete quasi-3-D analytical model of no-load magnetic field of double-sided slotted AFPMMs considering end effect," IEEE Access, vol. 6, pp. 59557 - 59566, 10 October 2018, doi: 10.1109/ACCESS.2018.2875306. (Article).

[12] K. D. Lee, J. Lee, and H. W. Lee, "Inductance calculation of flux concentrating permanent magnet motor through nonlinear magnetic equivalent circuit," IEEE Transactions on Magnetics, vol. 51, No. 11, pp. 1-4, 01 June 2015, doi: 10.1109/TMAG.2015.2438000. (Article).

[13] O. Taqavi, N. Taghavi, "Development of a mixed solution of maxwell's equations and magnetic equivalent circuit for double-sided axial-flux permanent magnet machines," IEEE Transactions on Magnetics, vol. 57, No. 4, 19 February 2021, doi: 10.1109/TMAG.2021.3060538. (Article)

[14] R. Alipour-Sarabi, Z. Nasiri-Gheidari, H. Oraee, "Development of a 3-D magnetic equivalent circuit model for axial flux machines," IEEE Transactions on Industrial Electronics, vol. 67, No. 7, 15 August 2019, doi: 10.1109/TIE.2019.2934065. (Article)

[15] B. Tak, J. Ro, "Analysis and design of an axial flux permanent magnet motor for in-wheel system using a novel analytical method combined with a numerical method," IEEE Access, vol. 8, pp. 203994 - 204011, 09 November 2020, doi: 10.1109/ACCESS.2020.3036666. (Article)

[16] E. Cetin, F. Daldaban, "Analyzing distinctive rotor poles of the axial flux PM motors by using 3D-FEA in view of the magnetic equivalent circuit," Engineering Science and Technology, an International Journal, pp. 1421-1429, 1 December 2017, doi: https://doi.org/10.1016/j.jestch.2017.11.008. (Article)

[17] W. Tong, S. Wang, S. Dai, S. Wu, R. Tang, "A quasi 3-D magnetic equivalent circuit model of a double-sided axial flux permanent magnet machine considering local saturation," IEEE Transactions on Energy Conversion, vol. 33, No. 4, pp. 2163–2173, 05 July 2018, doi: 10.1109/TEC.2018.2853265. (Article)

[18] A. Daghigh, H. Javadi, A. Javadi, "Improved analytical modeling of permanent magnet leakage flux in design of the coreless axial flux permanent magnet generator,"

Canadian Journal of Electrical and Computer Engineering, vol. 40, No. 1, 19 May 2017, doi: 10.1109/CJECE.2016.2550667. (Article)

[19] A. Hemeida, A. Lehikoinen, P. Rasilo, H. Vansompel, A. Belahcen, A. Arkkio, P. Sergeant, "A simple and efficient quasi-3D magnetic equivalent circuit for surface axial flux permanent magnet synchronous machines," IEEE Transactions on Industrial Electronics, vol. 66, No. 11, pp. 8318-8333, 09 December 2018, doi: 10.1109/TIE.2018.2884212. (Article)

[20] W. Jara, J. A. Tapia, N. Bianchi, J. Pyrhönen, R. Wallace, "Procedure for fast electromagnetic design of axial flux permanent magnet machines," International Conference on Electrical Machines ICEM, 02-05 September 2014, doi: 10.1109/ICELMACH.2014.6960364. (Conference Paper)

[21] Y.Kano, K.Tonogi, T.Kosaka, N.Matsui, "Torque-maximizing design of double-stator, axial-flux, pm machines using simple non-linear magnetic analysis," IEEE Industry Applications Annual Meeting, 23-27 September 2007, doi: 10.1109/07IAS.2007.137. (Conference Paper)

[22] A. Parviainen, "Design Of Axial Flux Permanent-Magnet Low Speed Machines And Performance Comparison Between Radial Flux And Axial Flux Machines", Thesis for the degree of Doctor of Science, Lappeenranta University of Technology, 2005.